Thermal effects of linked lithospheric and upper crustal–scale processes: Insights from numerical modeling of the Cenozoic Central Catalan Coastal Ranges (NE Spain)

M. ter Voorde,[1] J. M. Gaspar-Escribano,[1,2] J. Juez-Larré,[1] E. Roca,[3] S. Cloetingh,[1] and P. Andriessen[1]

Received 14 March 2007; revised 16 July 2007; accepted 20 August 2007; published 26 October 2007.

[1] Processes influencing the thermal state of the continental crust, such as heat upwelling related to rifting and isotherm reorganization due to mass redistribution by erosion, deposition, and (fault-)tectonic transport, operate at different scales, and their effects overlap. In this paper, we use lithospheric- as well as crustal-scale numerical modeling tools in order to quantify the contributions of these various factors to the geothermal field, establishing their relative relevance. We apply the models to address the thermal evolution of the Catalan Coastal Ranges (NE Spain) during the Cenozoic, a period that is characterized by a change in tectonic style, from Pyrenean compression to extension related to the western Mediterranean rifting. Results of the lithospheric-scale thermal model for extensional basins show an increase in the geothermal surface gradient of about 11°C/km in the Catalan Coastal Ranges during the Neogene, related to extensional thinning of the lithosphere in the Valencia Trough (western Mediterranean). Predictions of the upper crustal–scale thermal model, incorporating fault motions and surface mass redistribution (erosion and sedimentation), point to little changes in the isotherms due to fault block movements in the Paleogene and Neogene. In contrast, erosion appears to have a significant effect on the thermal history of basement rocks sited in the shallowest crust. Comparison of the integrated lithospheric- and upper crustal–scale modeling results with apatite fission track and apatite (U-Th)/He thermochronology data reveals larger amounts of Neogene to present cooling than predicted by the models. On the basis of this unresolvable mismatch, we suggest that, similar to present, forced fluid convection along fault planes played an important role in the evolution of the geothermal field during the Neogene stage of rifting. **Citation:** ter Voorde, M., J. M. Gaspar-Escribano, J. Juez-Larré, E. Roca, S. Cloetingh, and P. Andriessen (2007), Thermal effects of linked lithospheric and upper crustal–scale processes: Insights from numerical modeling of the Cenozoic Central Catalan Coastal Ranges (NE Spain), *Tectonics*, *26*, TC5018, doi:10.1029/2007TC002131.

1. Introduction

[2] The thermal evolution of an area undergoing tectonic deformation is influenced by numerous factors, operating at different spatial scales. Whereas thermal effects associated with changes in crustal or lithospheric thickness and mantle upwelling typically present long wavelengths (tens of kilometers and larger), other processes such as faulting, erosion and rock burial underneath the sedimentary cover, local magmatic intrusions (possibly containing radiogenic material) and fluid convection cause short-wavelength disturbances in the geothermal field (in the range of a few kilometers or even less).

[3] Numerous authors have addressed the effects of lithospheric stretching and of magmatism on the crustal thermal regime [e.g., *McKenzie*, 1978; *Vlaar*, 1983; *Durand*, 1984; *Morency et al.*, 2002], the cooling of rocks due to uplift accompanied by erosion [e.g., *Stüwe et al.*, 1994; *Rahn and Grasemann*, 1999; *Ring et al.*, 1999, *ter Voorde et al.*, 2004], as well as the impact of fluid circulation in the crustal geothermal field [e.g., *Drogue*, 1985; *Kukkonen*, 1995]. Yet, the combination of these regional- and local-scale thermal processes has received much less attention.

[4] The Catalan Coastal Ranges (CCR), located along the northeastern coast of Spain (Figure 1), constitute an ideal natural laboratory for a study of the interplay between thermal processes acting at different spatial scales: They can be regarded as a region of fault movements, on a scale of several tens of kilometers, but they also form a small part of a much larger system, as they are one of the flanks of the Valencia Through rift basin. Furthermore, an extensive data set for the CCR is available, including apatite fission track (AFT) and apatite (U-Th)/He (AHe) thermochronology data as well as independent constraints on the timing and magnitude of erosion. This combination of data eliminates the necessity of deriving erosion rates from thermochronological data, and thus gives us the opportunity to concen-

[1]Faculty of Earth and Life Sciences, Vrije Universiteit, Amsterdam, Netherlands.
[2]Now at Escuela Técnica Superior de Ingenieros Topografía, Geodesia y Cartografía, Universidad Politécnica de Madrid, Madrid, Spain.
[3]Facultat de Geologia, Universitat de Barcelona, Barcelona, Spain.

0278-7407/07/2007TC002131$12.00

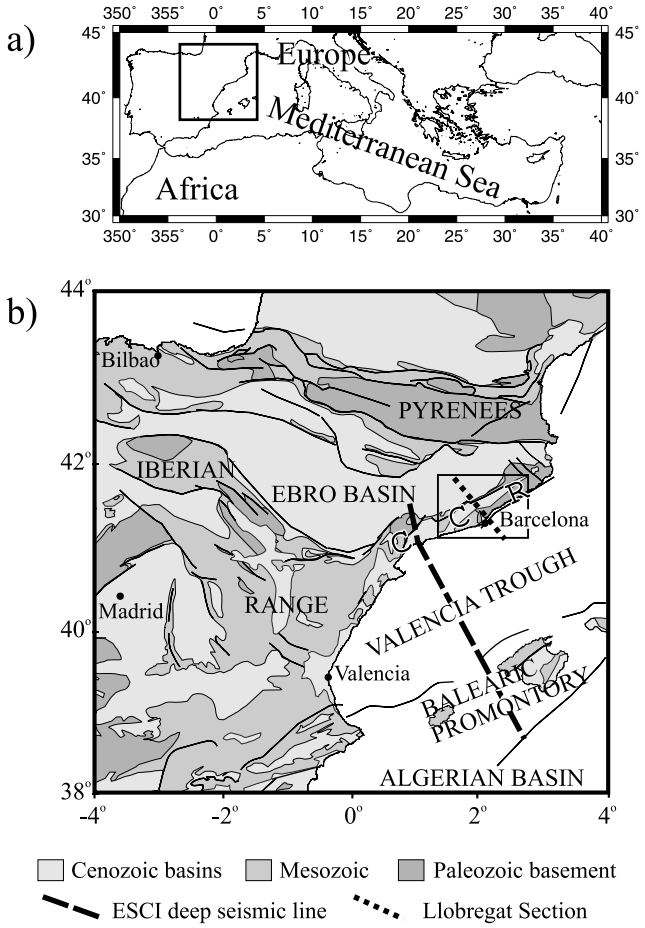

Figure 1. (a) Location map of the study area in the Mediterranean Sea. (b) Simplified geological map of NE Iberia indicating the location of the sections shown in Figures 2 and 3. CCR denotes Catalan Coastal Ranges.

trate on the processes affecting the thermal field of the continental crust.

[5] In this paper we assess the Cenozoic thermal evolution of the CCR by numerical modeling constrained by apatite fission track and apatite (U-Th)/He thermochronology. We compare the relative impact of the various processes that have an influence on the thermal field and quantify their contribution to the total thermal signal. Hereby we aim to increase our understanding of the interplay between factors influencing the thermal behavior of the continental crust at different scales.

1.1. Previous Work

[6] The CCR belong to a Paleogene slightly deformed intraplate contractional chain that was extensionally inverted during the Neogene. Earlier work on this Cenozoic evolution mainly dealt with the reconstruction of tectonic and surface processes [e.g., *Guimerà*, 1988; *Roca et al.*, 1999; *Gaspar-Escribano et al.*, 2001, 2004].

[7] Until recently, quantitative constraints on the thermal evolution of the CCR were limited to the Neogene extensional phase and mainly derived from lithospheric-scale modeling studies [e.g., *Fernàndez et al.*, 1990a; *Watts and Torné*, 1992; *Morgan and Fernàndez*, 1992; *Janssen et al.*, 1993; *Zeyen and Fernàndez*, 1994; *Negredo et al.*, 1999]. Actually, most of them aimed at describing the development of the Valencia Trough and gave only a secondary role to the CCR, which were merely regarded as the northwestern flank of this extensionally thinned basin. In addition to these large-scale models, some upper crustal–scale thermal modeling studies for the Neogene extensional configuration of the CCR are available, including basin-scale analyses of fluid convection systems generating thermal anomalies at present [*Fernàndez et al.*, 1990b; *Carmona et al.*, 2000; *Bitzer et al.*, 2001].

[8] The restriction of previous evolutionary studies to the extensional phase (late Oligocene–Miocene) was partly due to the very limited control on the preextensional geometry of the lithosphere in the CCR and on the amounts of uplift and erosion during the Paleogene compressive phase. However, results from recent tectono-sedimentary studies [e.g., *López-Blanco et al.*, 2000] and thermochronological studies [*Juez-Larré*, 2003; *Juez-Larré and Andriessen*, 2006], together with the ESCI-Catalanides deep seismic profile [*Gallart et al.*, 1994; *Vidal et al.*, 1998], provide new constraints for the thermal history of the CCR not only during the Neogene extensional phase but also during the Paleogene compressional phase.

1.2. Geological Setting and Tectonic Evolution

[9] The CCR extend over 250 km along the northeastern coast of Spain, between the Ebro Basin (southern foreland basin of the Pyrenees) and the Valencia Trough (Figures 1 and 2). They are part of the northeastern sector of the margin which separates the extremely thinned continental crust of the Valencia Trough from the relatively undeformed or thickened crust of the Iberian Plate. The CCR can be defined as a Paleogene fold-and-thrust system, mainly formed by longitudinal basement-involving thrusts, which was extensionally inverted during the opening of the Valencia Trough (late Oligocene–early Miocene), forming several horsts and grabens [e.g., *Roca et al.*, 1999].

[10] In their central part, the CCR are composed by two longitudinal mountainous chains, the Prelitoral and Litoral ranges, separated by the Vallès-Penedès Basin (Figure 3). The Prelitoral Range consists of a major Paleogene anticline with multiple NW-directed thrust sheets overthrusting the Ebro Basin. The Litoral Range is a Neogene horst structure tilted toward the NW and striking along the coast that does not show any noticeable Paleogene internal deformation. Between these two chains, the Vallès-Penedès Basin belongs to a half graben that developed along a major SE dipping normal fault (Vallès-Penedès Fault). The litoral horst is bounded to the SE by another major SE-dipping extensional fault (Barcelona Fault) which is parallel to the coast and separates it from the offshore Barcelona Basin (Figure 3).

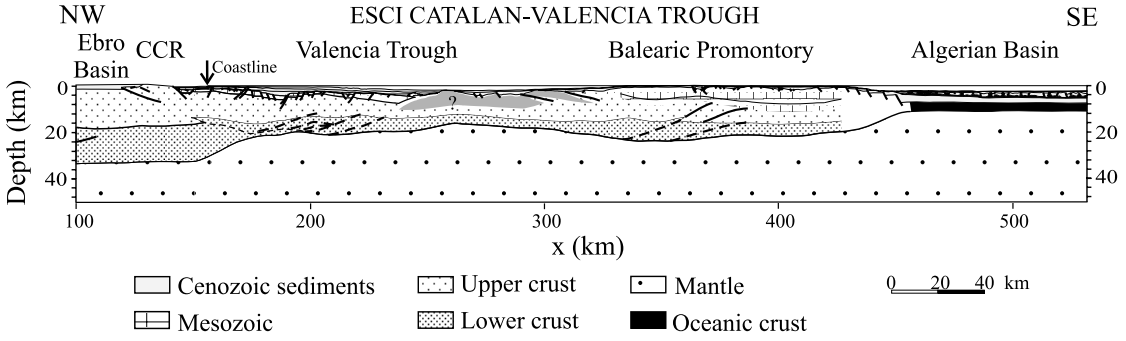

Figure 2. Interpreted lithospheric section across the Valencia Trough based on the ESCI Catalanides-Valencia Trough deep reflection seismic line (modified from *Roca* [2001]). See location in Figure 1b.

[11] The evolution of the Catalan Coastal Ranges during the Cenozoic can be divided into two stages [*Fontboté et al.*, 1990; *Roca*, 1996]: a Paleogene compressive stage and a Neogene extensional stage. During the Paleogene, N-S compressive stresses related to the development of the Pyrenean orogeny led to the inversion of the older Vallès-Penedès and Barcelona faults, which bounded previously formed Mesozoic basins [*Roca and Guimerà*, 1992]. This inversion was larger along the Vallès-Penedès Fault, resulting in the concentration of contractional deformation along the present-day Prelitoral Range (close to the Vallès-Penedès Fault). The amount of total shortening related to contractional deformation was only 7–15 km and did not induce significant crustal thickening (<2 km) [*López-Blanco et al.*, 2000; *Gaspar-Escribano et al.*, 2004]. The obliquity between the compressive direction and these older ENE-WSW-striking faults resulted in the development of a thick-skinned system of NNW-directed thrusts with a left-lateral strike-slip component which were restricted to upper crustal levels. During the development of these contractional faults, the region comprised between the Prelitoral Range and the offshore Barcelona Basin (referred to as the Catalan Intraplate Chain, CIC), was uplifted above sea level and underwent erosion [e.g., *Roca et al.*, 1999]. The resulting large amounts of synorogenic sediments were deposited into the Ebro Foreland Basin [e.g., *López-Blanco et al.*, 2000]. No magmatic activity has been reported for this stage.

[12] During the late Oligocene–Miocene, the opening of the Valencia Trough led to the extensional collapse of the CIC and a general rearrangement of the region into horsts and grabens [*Roca and Guimerà*, 1992], as it stands today (Figure 3). The onset of extension in the central CCR took place during the latest Chattian–earliest Aquitanian [*Parcerisa et al.*, 2007]. Whereas large parts of the CCR and adjoining Ebro basin areas were uplifted as a result of the Valencia Trough rift shoulder effect [e.g., *Gaspar-Escribano et al.*, 2001] and flexural unloading [e.g., *Gaspar-Escribano et al.*, 2004], extensional activation of the Barcelona and Vallès-Penedès faults governed the development of subsiding half-grabens in the Catalan margin [e.g., *Roca et al.*, 1999]. Effects of surface mass redistribution by erosion and sedimentation and subsequent isostatic readjustment of the lithosphere further contributed to shape the CCR [*Gaspar-Escribano et al.*, 2004]. Volcanic activity took place from early Miocene onward in the Valencia Trough, and from late Miocene onward in the area limiting the CCR to the NE [*Martí et al.*, 1992].

1.3. Modeling Strategy

[13] Taking into consideration the structural and tectonic evolution described above, the factors that are likely to have influenced the Cenozoic thermal evolution of the CCR are the Neogene lithospheric thinning event, normal and reverse faulting, and mass redistribution by erosion and sedimentation. Since these processes act at different scales, we approach the problem from a two-folded perspective, implying that we analyze the Cenozoic thermal evolution of the CCR area in two different spatial scales separately.

[14] In the first part of this study, large-wavelength changes in the thermal field associated with lithospheric thickness variations are analyzed. Since Paleogene contractional deformation did not produce any significant large-wavelength change in the lithospheric structure of the region and therefore of the lithospheric thermal regime, this analysis has been restricted to the Neogene extension when crustal and lithospheric thicknesses decreased considerably. The significance of the rift-related thermal disturbance for the thermal structure of the CCR is derived from the results of a lithospheric-scale thermal model.

[15] In the second part of the study, short-wavelength thermal changes are analyzed from an upper crustal–scale model which integrates fault motions, sedimentation and erosion with thermal calculations and ignores the stretching event. In this shallow domain, we have good control on the parameters describing the deformation, such as fault geometry and periods of fault activity.

[16] Finally, the results of the regional- and local-scale modeling will be combined, and compared to the recently obtained AFT and AHe data [*Juez-Larré*, 2003; *Juez-Larré and Andriessen*, 2006].

2. Inferences From Aft and U-Th/He Data

[17] The combination of apatite fission track and (U-Th)/He thermochronology is a unique method to unravel the thermal evolution of rocks in the uppermost continental crust at very

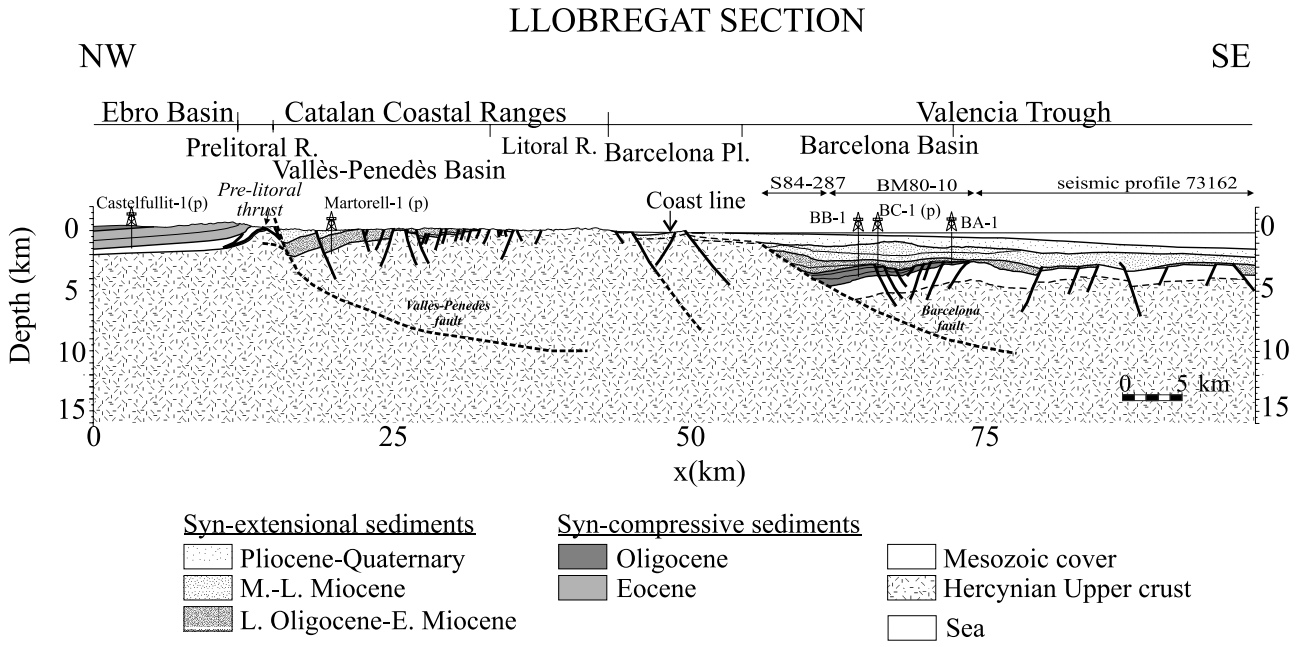

Figure 3. Llobregat Section: interpreted structural cross section across the central CCR along the Llobregat river (modified from *Gaspar-Escribano et al.* [2004]). There is no vertical exaggeration. Thick dashed lines depict the inferred deep geometry of the faults; (p) denotes projected well. S84-287, BM80-10, and 73162 refer to commercial reflection seismic profiles. See location of the section in Figure 1b.

low temperatures (40°–120°C) [e.g., *Gallagher et al.*, 1998; *Ehlers and Farley*, 2003]. Thermal histories reconstructed by means of this methodology provide information on the most recent changes in the geothermal gradient and/or the exhumation histories of rock samples. For the Litoral and Prelitoral ranges, AFT and AHe studies have been carried out and extensively described by *Juez-Larré* [2003] and *Juez-Larré and Andriessen* [2002, 2006]. Their findings are used in this study to constrain and discuss our numerical modeling results.

[18] The thermochronological results used for comparison with our modeling results are derived from the late Hercynian granitic basement samples collected along the Litoral and Prelitoral ranges (see Figure 4). Apatite fission track analysis yielded ages between 223 ± 27 Ma and 21 ± 3 Ma and mean track lengths (MTLs) between 11.3 ± 0.2 and 13.5 ± 0.2 μm. (U-Th)/He analysis yielded ages between 58 ± 3 Ma and 2.0 ± 0.2 Ma [*Juez-Larré and Andriessen*, 2006]. Inverse modeling was used to reconstruct the thermal evolution of the samples from the AFT age and length distribution. To this purpose, the software AFTSolve [*Ketcham et al.*, 2000] was used with the annealing model for Durango of *Laslett et al.* [1987], since microprobe analyses characterized the apatite from the basement as F-Cl apatites [*Juez-Larré*, 2003]. The results allow constraining the regional tectono-thermal history of the Central CCR for the Cenozoic as well as for the Mesozoic.

[19] For the Cenozoic, the thermal evolution of the sampled rocks is linked in time with the Paleogene compressive building of the CIC and the Neogene extensional opening of the Valencia Trough [*Juez-Larré*, 2003]. AFT and AHe data show no evidence for substantial rock cooling during the Paleogene compression. Rock samples [4], [67], [77], [110] and [135] (Figure 4), are characterized by pre-Neogene (mostly Mesozoic) AFT ages and relatively low MTLs (11.3 ± 0.2–12.8 ± 0.1 μm). During the Neogene extension, samples with AFT ages ranging between 31 ± 4 Ma and 21 ± 3 Ma and high MTLs (>13.2 ± 0.2 μm), all located in footwall blocks of major normal faults and close to these faults, show fast cooling (>4°C/My) across the apatite Partial Annealing Zone (PAZ).

3. Lithospheric-Scale Thermal Modeling

3.1. Neogene Thermal Evolution

[20] A lithospheric-scale, forward kinematic model for basin extension [*Kooi et al.*, 1992] has been applied in order to provide a first-order description of the thermal structure of the lithosphere in the Valencia Trough and adjoining areas, and particularly of the temporal variation of the geothermal gradient in the CCR. In this model, the thermal structure of the lithosphere is calculated assuming heat conduction and advection in both vertical and horizontal directions. Constant temperatures at the surface and at the base of the model are taken as boundary conditions. Rifting is simulated by imposing a gradual thinning of the lithosphere during the syn-rift stage, around a so-called 'necking level' that remains horizontal in the absence of isostatic forces. The thinning factors can laterally be varied by the

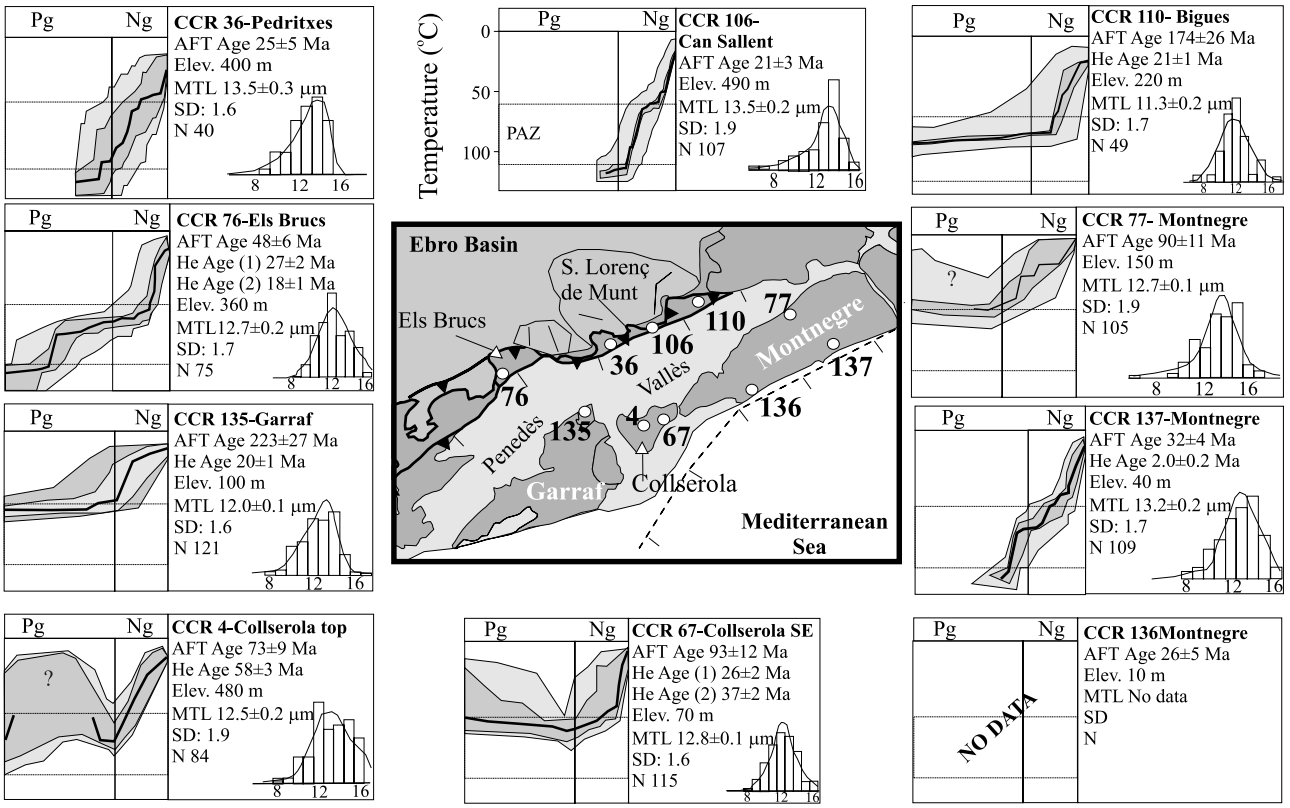

Figure 4. Apatite fission track data for the central and northern CCR [after *Juez-Larré and Andriessen*, 2006]. In the center is shown a location map of AFT samples (white dots) (framed area in Figure 1b). Surrounding plots show temperature-age diagrams calculated with the software AFTSolve [*Ketcham et al.*, 2000], using the annealing model for Durango of *Laslett et al.* [1987]. Grey shading corresponds to the error envelopes for each best-fitting thermal history (black line) satisfying the AFT data (dark gray, good fit; light gray, acceptable fit). Pg, Paleogene; Ng, Neogene; PAZ, Partial Annealing Zone for the apatite fission track thermochronometer. Boxes at the right show sample names, AFT ages and in some cases AHe ages, elevations of the sample (in meters a.s.l.), AFT mean track lengths (MTL; in μm) with standard deviations (SD), and numbers of apatite fission tracks length measurements (N) and the corresponding track length distribution histograms (horizontal scale is μm).

user of the model. In each model time step, the isotherms adapt to the new lithospheric configuration, initially rising as the lithosphere is stretched and subsequently relaxing as a result of lateral and vertical conductive heat transfer.

[21] The modeled section is based on a deep reflection seismic line crossing the Valencia Trough and CCR and constrained by wide-angle and ESP data (Figure 2) [*Sàbat et al.*, 1997; *Vidal et al.*, 1998; *Gaspar-Escribano et al.*, 2003]. The amount of thinning was predefined by setting different stretching factors for crust (β_C) and subcrustal lithosphere (β_M). The first one was derived by dividing the estimated initial crustal thicknesses (32 km) by the observed crustal thickness, which in principle did not change significantly during the postrift phase [e.g., *Roca*, 2001]. Since the lithosphere-asthenosphere boundary is defined by an isotherm, the stretching factors for the subcrustal lithosphere could not be measured directly, but were obtained by trial-and-error, i.e., adjusting them until the predicted present-day 1300°C isotherm corresponded with its observed position, as given by *Ayala et al.* [1996]. Other modeling parameters are listed in Table 1. For more details on the lithospheric-scale model the reader is referred to *Gaspar-Escribano et al.* [2003].

[22] Figure 5 shows the predicted thermal structure of the lithosphere in six successive time frames. The situation before rifting (Figure 5a; 25 Ma) is assumed to consist of a 100-km-thick lithosphere with a constant geothermal gradient of 13.3°C/km (resulting from the assumed base temperature of 1330°C). The subsequent thinning is set to occur around a necking level of 15 km; above this depth crustal material moves downward and not upward. As rifting proceeds, asthenospheric material ascends, implying an upward displacement of the isotherms. This causes an increase in geothermal gradient which is most pronounced in the axial zones of the basin, where the lithosphere is thinned some 60 km. The heating attains its maximum intensity at the end of the main stretching pulse (Figure 5c; 15 Ma). Subsequently during the postrift stage (15–0 Ma),

Table 1. Lithospheric-Scale Modeling Parameters Based on Work by *Gaspar-Escribano et al.* [2003]

Parameter	Value	Source[a]
Initial thickness of the crust	32 km	(1)
Initial thickness of the upper crust	16 km	(2)
Initial thickness of the lithosphere	100 km	(3)
Initiation of rifting	25 Ma	(3)
Duration of rift phase	9 Ma	(3)
Sediment density (grain density)	2600 kg m^{-3}	adapted from (4)
Crustal density (average)	2825 kg m^{-3}	(4)
Density of the mantle	3270 kg m^{-3}	(4)
Surface porosity	0.75	derived from (5) and (6)
Depth-porosity relation constant	0.55 m^{-1}	(5)
Temperature at the base of the lithosphere	1330°C	(7)
Thermal diffusivity	$7.8 \cdot 10^{-7}$ m^{-2} s^{-1}	(7)
Thermal expansion coefficient	$3.4 \cdot 10^{-5}$ °C	(7)

[a]Sources: (1) *Banda* [1988]; (2) *Roca* [2001]; (3) *Pino and Helmberger* [1997]; (4) *Watts and Torné* [1992]; (5) *Clavell and Berástegui* [1991]; (6) *ter Voorde et al.* [1998]; (7) *Kooi et al.* [1992].

the lithosphere experiences a gradual but not complete thermal relaxation (Figure 5f; 0 Ma).

[23] The curved shape of the 1300°C isotherm underneath the CCR, and the extreme thinning in the axial part of the Valencia Trough are satisfactorily reproduced by our large-scale modeling results. Also the predicted midcrustal temperatures are in agreement with previous modeling studies adopting flexure and predefined stretching factors [*Watts and Torné*, 1992], local isostasy and constrained by thermal and gravity data [*Zeyen and Fernàndez*, 1994], intracrustal decoupling level with differential motion of upper and lower crust [*Negredo et al.*, 1999] and joint 3D geoid and gravimetric anomalies modeling [*Ayala et al.*, 1996, 2003].

3.2. Surface Thermal Gradient in the CCR

3.2.1. Results

[24] The calculated thermal effect of the Neogene lithospheric thinning of the Valencia Trough in the upper crust of the CCR can most conveniently be represented by the temporal variation of the geothermal gradient. The changes in the thermal state of the crust in the CCR induce a temporal variation of the surface thermal gradient, which we measured in the model by calculating the gradient in the uppermost 5 km of the crust (Figure 6a). Our modeling results predict an increase of the surface gradient of 11 ± 1°C/km (i.e., from 13° to 24°C/km).

[25] A large portion (±6°C/km) of this increase is derived to take place during the postrift phase. This is due to the high modeled rate of subcrustal thinning, implying that conduction cannot keep up with advection. The system needs some extra time to transport the heat to the surface,

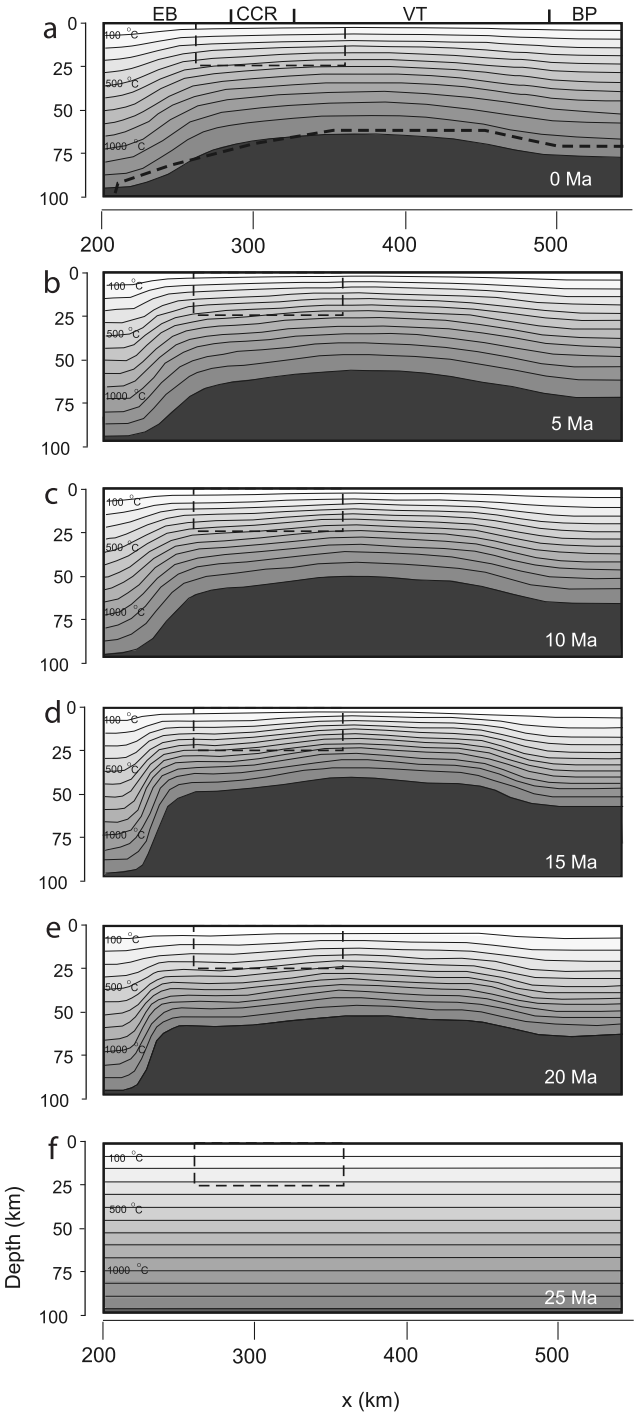

Figure 5. Thermal structure across the Valencia Trough predicted by the lithospheric-scale model. From bottom to top are shown prerift (25 Ma), syn-rift (20 and 15 Ma), and postrift (10, 5, and 0 Ma) stages. Contour lines each 100°C. EB, Ebro Basin; CCR, Catalan Coastal Ranges; VT, Valencia Trough; BP, Balearic Promontory. Location of the section as in Figure 1b, but excluding the Algerian Basin. Thick dashed line in present-day section indicates the lithosphere-astenosphere boundary as derived by *Ayala et al.* [1996]. Thin dashed box indicates the upper crustal–scale modeled area of Figure 8.

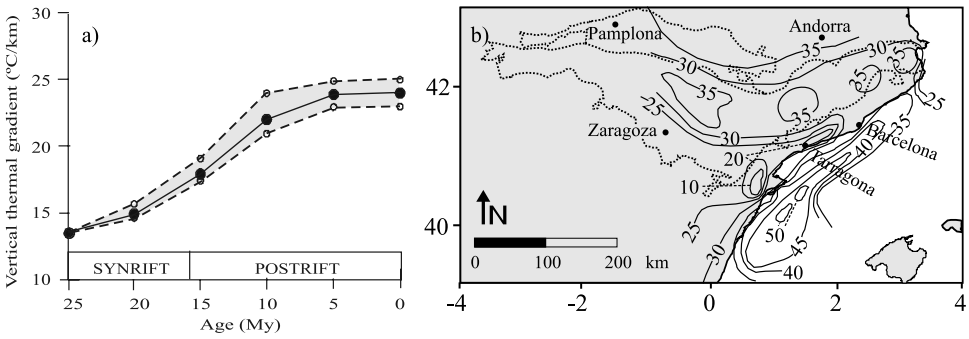

Figure 6. (a) Average geothermal gradient as a function of time, predicted by the lithospheric-scale thermal model for the upper 5 km of the crust of the CCR domain (x = 310 km in Figure 5). Dashed lines denote maximum and minimum thermal gradients in a horizontal distance range of 20 km. (b) Present-day surface thermal gradient map of the study region (modified after *Fernàndez et al.* [1990a]). Isolines are each 5°C/km.

as can be shown by estimating the Peclet number, *Pe*. The Peclet number is defined as $Pe = v \cdot h/k$, where v is the rate of advection, h the 'typical length scale', for example the distance from the Moho to the surface, and k the thermal diffusivity, and indicates whether advection dominates (Pe > 1) or conduction (Pe < 1). Taking v = 6.3 mm/a (which is the rate of uplift of the asthenosphere-lithosphere boundary beneath the CCR resulting from the model), h = 32 km and $k = 10^{-6}$ mm^2/s, we obtain that Pe = 6.4, demonstrating that advection is more significant that conduction.

3.2.2. Sensitivity Analysis

[26] To test the sensitivity of the obtained result to the imposed thinning factors, we repeated the model run with different values for subcrustal lithosphere thinning.For this sensitivity test, we calculated β_M by dividing the prerift subcrustal lithospheric thickness by its present-day value. The effect is that the predicted 1300°C isotherm immediately after the syn-rift phase corresponds with the observed present-day position of the lithosphere-asthenosphere boundary, but subsequently moves to a greater depth owing to thermal relaxation [see *Gaspar-Escribano*, 2003, Figure 5.1]. This scenario yields a significant underestimation of β_M and generates a lithosphere-asthenosphere boundary that is at maximum 25 km deeper than the observed one. Nevertheless, the difference in the surface thermal gradient between the two modeled scenarios turned out to be not more than 1°C/km. This can be explained by the fact that we measure the surface gradient in the upper 5 km, i.e., above the necking depth. This layer is influenced by changes in subcrustal lithospheric thinning only by the effect of heat conduction, and not by the effect of heat advection.

3.2.3. Comparison With Earlier Work

[27] The predicted values of around 24°C/km for the present-day surface gradient are lower than the measured background thermal gradient of the area (30 to 35°C/km, which are values corrected for short-wavelength anomalies produced by groundwater convection [*Fernàndez and Banda*, 1989; *Fernàndez et al.*, 1990a], Figure 6b). This can be explained by the neglect of radiogenic upper crustal heat production in our model: Inclusion of heat production would cause a higher modeled upper crustal gradient and a slightly smaller increase of this gradient due to crustal thinning. Nevertheless, in the CCR domain the temporal change in the thermal gradient due to lithospheric thinning would hardly change, since the thickness of the heat producing layer in the this area remained effectively the same (remember that crustal thinning (βc) in the model was different form mantle thinning (βm)).

[28] Therefore we conclude that an increase in the thermal gradient of 11 ± 1°C/km can be regarded as a reliable representative for the thermal effect produced by the Neogene thinning of the Valencia Trough lithosphere on the CCR. This increase in gradient will be combined with the upper crustal–scale modeling results shown in the next sections.

4. Upper Crustal–Scale Model: Model Description and Some Synthetic Results

4.1. Model Description

[29] For the analysis of small wavelength disturbances that influence the thermal field, we have used a crustal-scale kinematic model, integrating fault motions, sedimentation and erosion with thermal calculations [*ter Voorde and Bertotti*, 1994; *ter Voorde et al.*, 2004]. In this model, fault blocks are defined in the upper crust, separated from the lower part of the model by a midcrustal detachment level in which faults flatten out. In the lower lithosphere, deformation is assumed to be more gradually distributed. The faults can be activated independently from each other, and at different rates in different periods. Mass transport along the fault planes is set to occur following a vertical shear mechanism. Sea level variations can be imposed as input parameter in the model. Also, topographic and bathymetric profiles can be prescribed by the model user for several instants in time, and implies erosion of all material located above these profiles and infill by sediments of the space below them (similar to the ''mathematical erosion'' of *Rahn*

Table 2. Upper Crustal–Scale Thermomechanical Parameters[a]

Magnitude	Value (Unit)
Surface temperature	10°C
Temperature base lithosphere	1330°C
Thermal diffusivity	$1 \cdot 10^{-6}$ $m^{-2}s^{-1}$
Heat production	$4.8 \cdot 10^{-6}$ Wm^{-3}
Thickness heat-producing layer	10 km
Specific heat	1100 J $kg^{-1}K^{-1}$
Thermal expansion coefficient	$3.4 \cdot 10^{-5}$ K^{-1}
Thickness brittle layer	16 km
Depth to detachment	16 km
Sediment density	2000 kg m^{-3}
Crustal density	2850 kg m^{-3}
Subcrustal lithospheric density	3250 kg m^{-3}
Initial crustal thickness	32 km
Initial lithospheric thickness	100 km

[a]Thermal parameters after *ter Voorde* [1996], initial crustal thickness after *Banda* [1988], initial lithospheric thickness after *Pino and Helmberger* [1997]; densities after *Gaspar-Escribano et al.* [2003].

and Grasemann [1999]). Boundary conditions of the model are top and bottom temperatures, the shape of the surface isotherm being corrected every time step according to the imposed topography/bathymetry profiles. The values of the top and bottom temperature cannot be varied over time.

[30] For each numerical time step, the model calculates the new crustal configuration and topography, as well as the new thermal field and related density contrasts. For the temperature calculations, heat transport by conduction and advection is considered, as well as radiogenic heat production. (Note that advection is here defined as heat transport caused by displacement of crustal material, dragging the enclosed heat with it as it moves, and that effects of fluid circulation are not included in this model.)

[31] The new load distribution resulting from mass transport, erosion and/or sedimentation, and thermal readjustment is compensated isostatically, according to a thin-plate elastic model. Model outputs are the geometry of the section and the thermal structure of the crust in each time step, as well as thermal histories of given synthetic rock samples, moving with the crustal material.

4.2. Synthetic Modeling: The Influence of Faulting on the Gradient in the Footwall Block

[32] Tectonic rearrangement of the crust by fault activity affects the distribution of the isotherms and implies a change in the geothermal gradient. In the vicinity of master faults heat advection caused by the displacement of crustal fault blocks might have a prime control on the thermal field, but it has been shown that this only is perceptible for rapid fault slip rates [*Grasemann and Mancktelow*, 1993; *ter Voorde and Bertotti*, 1994; *Ehlers and Chapman*, 1999]. To test the significance of the rate of compression or extension as a parameter modifying the geotherm for the setting of the CCR, a simple synthetic model including one fault and no sediment transport was designed. Fault dimensions and order of magnitude of the tested rates of fault displacement were chosen to reflect the situation in the CCR, in order to be able to extend our conclusions to the specific case of this area. The thermal parameters used are given in Table 2. Results of our analysis are given in Figure 7 and show that in footwall domains (where thermochronological constraints are available) an increase in fault displacement velocities of as high as a factor 10 causes an increase in thermal gradient of only up to 5°C/km. From this, we can conclude that faulting has a very limited

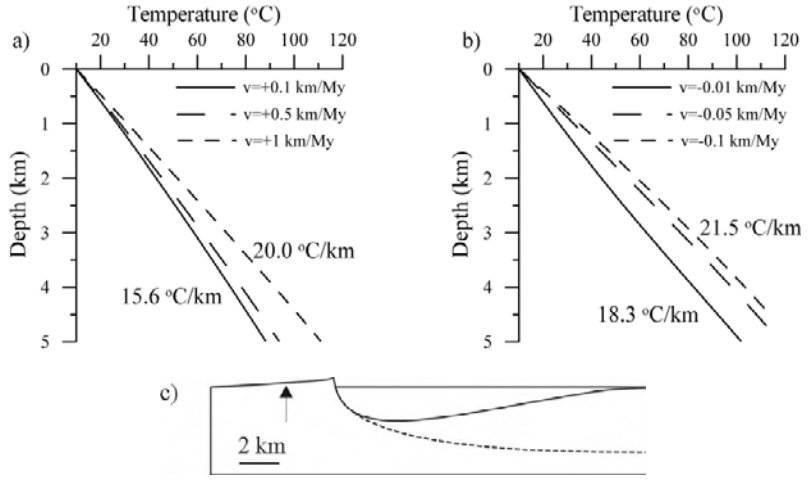

Figure 7. Results from synthetic modeling with neither erosion nor deposition on the footwall and only one fault moving at velocity v, showing the thermal gradient calculated in the footwall block at a horizontal distance of 2 km from the fault after 26 Ma, for (a) extension and (b) compression. (c) Schematic section, indicating the position of the measured thermal gradient. Note that the basin is filled with sediments up to the surface.

Table 3. Fault Kinematics[a]

Fault	t_i	t_f	v_h	Δx
Th1	54	49	−0.34	−1.7
Th2	41	29	−0.48	−5.8
BCNf	28	15	0.55	+7.2
	15	6	0.2	+1.8
VPf	28	6	0.17	+3.7

[a]Notation: t_i, time of activation of fault (Ma); t_f, time of cessation of fault activity (Ma); v_h, horizontal velocity (minus for compression, plus for extension); Δx, horizontal displacement in direction of movement (minus for shortening, plus for extensional displacement).

influence on the temperature of rock samples in the CCR. Changes in temperature-time curves calculated by the upper crustal–scale model in the next section should therefore be attributed to other factors such as erosion.

5. Upper Crustal–Scale Modeling of the Catalan Coastal Ranges

5.1. Input Data

5.1.1. Fault Geometry and Kinematics

[33] Present-day fault geometries are constrained at a basin scale by reflection seismic data [*Bartrina et al.*, 1992; *Roca et al.*, 1999]. Extrapolation of deep seismic profiles in adjacent regions (southwestern CCR [*Sàbat et al.*, 1997; *Roca et al.*, 2004]; Figure 2) and restoration studies [*Roca and Guimerà*, 1992; *Gaspar-Escribano et al.*, 2004] indicate a listric geometry for the extensional faults, which sole out at depths between 10 and 16 km in a detachment level (Figure 3). More difficult to assess is the geometry of thrust faults that were active during the Paleogene compressive stage. Only surface geological studies provide some constraints in this respect [*López-Blanco et al.*, 2000; *López-Blanco*, 2002]. According to these authors, three major compressional stages could be distinguished, based on the particular modes of deformation. The first stage, early middle Eocene, is characterized by the development of a thick-skinned thrust system northwestward of the present-day Vallès-Penedès Fault. Its geometry is consistent with the reactivation of a former (Mesozoic) extensional fault which coincided in depth with the present Vallès-Penedès Fault (Th1 in Table 3). Subsequently, during the second stage (middle Eocene in age), the deformation style switched to the growth of a fault-progradation fold in the same area. The related thrust ramp is inferred to have a lower dip. However, since the surface expression of this fault is unknown (it should be buried beneath the Vallès-Penedès Basin fill) and related displacement is supposed not to be significant, it is not included in the model. Finally, when the fault-progradation fold attained a critical state, the third stage is characterized by the emplacement of an out-of-sequence thrust (Th2 in Table 3). This thrust crosscuts all previous structures and causes uplift of the basement during the middle Eocene–early Oligocene.

5.1.2. Mode of Isostatic Compensation and Thermal Parameters

[34] Regional isostasy was applied in the upper crustal–scale model in order to compensate changes in lithospheric loading. Appropriate values were derived in earlier studies [*Gaspar-Escribano et al.*, 2001, 2004]. The flexural rigidity was set to a value of $9.7 \cdot 10^{22}$ Nm (equal to an effective elastic thickness T_e of 25 km) in the Ebro Basin ($x <$ 10 km in Figure 8; Present-day) and was assumed to decrease linearly to 10^{21} Nm ($T_e \sim 6$ km) across the area corresponding to the CCR (between $x = 10$ km and $x =$ 50 km). This last value was kept constant across the whole Valencia Trough ($x > 50$ km). The detachment level where the major faults sole out was set at a depth of 16 km [*Gaspar-Escribano et al.*, 2001, 2003]. These and the thermal parameters, which were assumed to have standard values (see, e.g., *ter Voorde* [1996] for discussion), are listed in Table 2.

5.1.3. Initial Topography

[35] The topography at the onset of modeling (55 Ma) was assumed to be flat, which is in accordance with the following observations.

[36] 1. The sedimentary record in Garraf denotes that during Late Cretaceous the area of the CCR was covered with widespread shallow water carbonates, indicating that the topography was almost flat and near sea level.

[37] 2. During latest Cretaceous and Palaeocene, the sedimentary record reveals a generalized uplift of the CCR with development of paleosoils and karstified surfaces that were covered during the Palaeocene by red mudstones (Mediona formation) with several paleosoil levels. This uplift, present in almost all the Iberian Peninsula was surely minor since there is not an angular unconformity between the Palaeocene and the Upper Cretaceous (excepting some very local unconformities which are only observed 100 km southward in the Maestrat Basin), and the Palaeocene in the Ebro Basin, CCR and Balearic Islands does not include detrital rocks denoting the presence of high reliefs in the surrounding areas.

[38] Accordingly, the initial topography of CCR of the model must have been positive but probably less than 200 m.

5.1.4. Palaeotopography, Amounts of Erosion, and Sedimentation

[39] Ideally, first-order estimates of amounts of erosion and sedimentation can be derived from sediment budget

Figure 8. Upper crustal–scale modeling results: thermal structure in five representative times. Dashed and solid lines represent inactive and active faults, respectively. Black dot, location of litoral synthetic sample; white square, location of prelitoral synthetic sample; EB, Ebro Basin; PR, Prelitoral Range; VP, Vallès-Penedès Basin; LR, Litoral Range; BB, offshore Barcelona Basin.

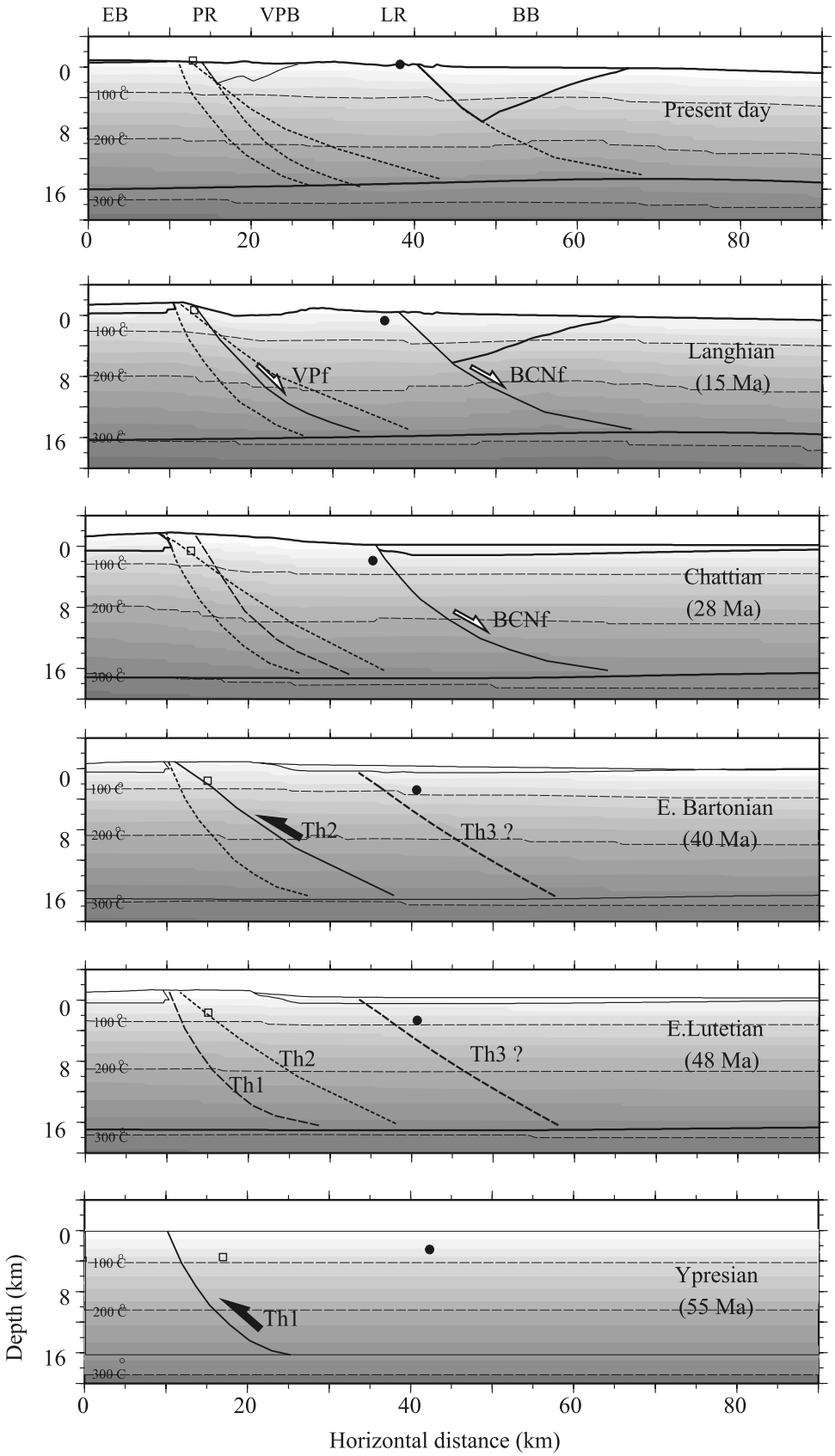
EB
PR
VPB
LR
BB
Present day
Langhian
(15 Ma)
VPf
BCNf
Chattian
(28 Ma)
BCNf
E. Bartonian
(40 Ma)
Th2
Th3 ?
E.Lutetian
(48 Ma)
Th2
Th3 ?
Th1
Ypresian
(55 Ma)
Th1
100 C
200 C
300 C
0
8
16
0
20
40
60
80
Depth (km)
Horizontal distance (km)

Figure 8

calculations in partially restored sections, assuming that the area of the sedimentary infill of the grabens is equal to the area of rocks removed by erosion from the source areas. However, this approach relies on some severe assumptions: It implies that all the material eroded from elevated areas was deposited and remained in the basins, and therefore is only accurate for periods during which the basins were closed systems, without out-of-plane transport. Furthermore, these calculations also assume that sediment and source rock densities are similar, which is usually not the case. As in general densities of the eroded rocks are larger than densities of the sediments, the volume of rocks accumulated in the basin constitutes an upper bound for the total volume of rocks eroded in the source area. The Cenozoic evolution of the CCR included several stages in which out-of-plane transport was relatively significant. For these periods, the abovementioned conditions are not properly satisfied, implying that a sediment budget calculation provides only a very limited amount of constraints for this study.

[40] Nevertheless, some very raw estimates for amounts of erosion were made in an earlier study [*Gaspar-Escribano*, 2003] resulting in a maximum average of 2.2 km of erosion for the Prelitoral Range during Chattian-Tortonian, and of 0.8 km for the CIC during Ypresian–late Rupelian. The following additional constraints from independent sedimentary studies were also used in the model [see *Gaspar-Escribano et al.*, 2004].

[41] 1. Late Eocene palaeotopography locates the Ebro Basin around 1 km lower than the frontal part of its catchment area (the CIC), as indicated by paleobotany, structural reconstructions and analyses of erosional products deposited in the Ebro Basin fans of Sant Llorenç de Munt and Montserrat [*López-Blanco et al.*, 2000]. Additionally, accumulation of marine to continental Eocene–lower Oligocene deposits in offshore areas (Barcelona and Sant Feliu basins) and close to the present coastline (CIC hinterland) indicates that the eroding catchment areas were restrained between the Ebro Basin and the present Mediterranean coastline [*Roca et al.*, 1999; *López-Blanco et al.*, 2000]. Furthermore, clast composition and volume of these Eocene fans, roughly consisting of up to 80% of originally Triassic rocks [*Marzo and Anadón*, 1988; *López-Blanco et al.*, 2000], suggests that the ~0.8-km-thick layer of Triassic series and in a less degree Hercynian basement were eroded over this wide area.

[42] 2. For the late Oligocene–Neogene extensional stage, water depth estimates from *Roca and Desegaulx* [1992] are used to constrain the SE part of the section (present-day offshore). The early middle Miocene (19–14 Ma) marine episode recorded in some parts of the Vallès-Penedès Basin [*Cabrera and Calvet*, 1996] indicates that this part of the section was located at sea level.

[43] On the basis of these constraints, topography/bathymetry profiles were constructed for different times to reproduce erosion and deposition in the model. During the modeling, these profiles were iteratively adjusted in order to fit the more rigid geological constraints as basin and mountain configuration and amounts of erosion. Finally, they were corrected in vertical coordinate for relative sea level changes adopting the curve of *Haq et al.* [1987].

5.2. Upper Crustal Modeling Procedure

[44] We modeled the section crossing the central CCR (Figure 3), with a simulated time span of 55 Ma (Paleocene to Present). The initial topography was set to zero and thermal and elastic parameters were set constant throughout the model evolution. Initial fault geometries as well as rates and duration of fault activity were modified in repeated model runs, until a good fit was obtained between modeling results and geological data for the past and present-day geometries of basins and mountains. Subsequently, calculated thermal histories of synthetic samples located in Litoral and Prelitoral ranges were compared with those derived from AFT analyses with the objective of reproducing the same cooling or heating trends. Thermal histories calculated by the model strongly depend upon two factors that were varied to refine the results: (1) amounts of erosion and sedimentation imposed via topography-bathymetry profiles (section 5.1.4); and (2) depth of the sample below the free surface at the beginning of the model. Variations of these parameters were restricted to satisfy independent estimates on palaeoelevation, erosion and sedimentation as well as to make the sample be located at the Earth's surface at the end of the model run.

5.3. Upper Crustal–Scale Modeling Results

5.3.1. Kinematic Evolution

[45] Figure 8 shows the evolution of basins and mountain belts geometry resulting from the model. During the initial stage (55–49 Ma), the thrust recording the inversion of the older Mesozoic extensional fault located close to the present-day Vallès-Penedès Fault (referred to as Th1) developed, deforming the surface in its frontal parts. The topography resulting from the combined effects of this compressive deformation and erosion attained up to 1 km, as represented by the model (Figure 8, Early Lutetian). This stage was followed by the formation of the not modeled major fault progradation fold in the Prelitoral Range (48–42 Ma).

[46] Subsequently and according to the model, the motion of the out-of-sequence thrust (Th2) resulted in the widening southeastward of the uplifted area until near ~30 km (Figure 8, Early Bartonian). Also during this last compressive stage, the CIC reached its maximum elevation with calculated values as high as 1.7 km (Figure 8, Chattian). Erosional unroofing of this relief caused the shedding of large amounts of syn-orogenic sediments toward the NW into the Ebro Basin and to minor degree toward the SE into the hinterland (present-day Barcelona Basin), quantified by the model as up to 1.5 km and up to 0.8 km, respectively.

[47] The tectonic inversion of major Paleogene faults initiated during the late Oligocene (Figure 8, Chattian) and led to the partitioning of the CIC into a horst-and-graben system (Figure 8, Langhian). Vertical motions (uplift and subsidence) were accentuated during this period because of the higher deformation rates and steeper fault dips (section 4.2 and Table 3). Whereas normal faulting

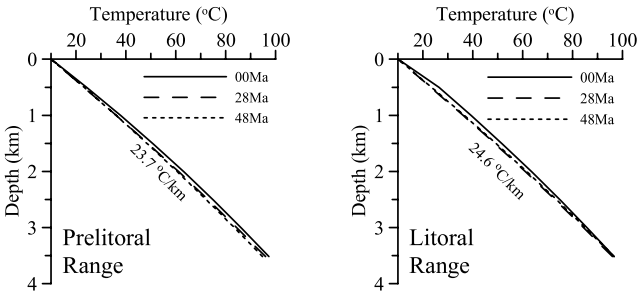

Figure 9. Geothermal gradient predicted for two locations shown in Figure 8 (corresponding to the prelitoral and litoral ranges). Numbers indicate calculated mean geothermal gradient for the uppermost 5 km of the crust.

(BCNf and VPf) led to destruction of previously formed topography, flexural rebound in their footwall blocks, enhanced by substantial erosional unloading, contributed to the uplift of the Litoral and Prelitoral ranges and of the Ebro Basin. For a more in-depth discussion on the evolutionary, kinematic modeling of the CCR, the reader is referred to *Gaspar-Escribano et al.* [2004].

5.3.2. Thermal Evolution

[48] The modeled evolution of the thermal field, depicted in Figure 8, does not show major thermal changes in the upper crust caused by Cenozoic fault block movement. The geothermal gradients calculated in two representative locations of the present-day Prelitoral and Litoral ranges (Figure 9) are rather constant throughout the modeled Cenozoic evolutionary stages (~24°C/km in the uppermost 4 km of the crust) with only slight fluctuations, within a range of 3°C/km. Also, in all modeled evolutionary stages, the uppermost isotherms follow the topographic profile with little deviations, and the base of the competent brittle crust (initially at depth of 16 km) roughly corresponds to the 275°–300°C isotherms (Figure 8). This lack of significant changes in the thermal field is related to the fault movement velocities used in the model, which are not high enough to cause strong changes in the isotherms (see section 4.2).

[49] Nevertheless, some minor thermal differences can be observed between the Paleogene compressive and Neogene extensional stages within this rather uniform thermal scenario. Whereas the thermal structure of the upper crust during the compressional stage (55–29 Ma) only shows smooth lateral variations, during the extensional phase (28–0 Ma) those are more significant and concentrated around fault planes and at shallow levels within the range of AFT detection. More precisely, during extension, the isotherms are shown to have been pulled downward in the Vallés-Penedès Basin and upward in the Litoral Range, Prelitoral Range and adjacent Ebro Basin areas.

6. Thermal Signal: Combining the Scales

6.1. Thermal and Exhumation Histories of Basement Units

[50] We have monitored the exhumation and thermal history of two synthetic basement samples, representing a Prelitoral and a Litoral Range evolution. Their position at the end of the modeling was at the surface, requiring initial burial depths of 3.6 and 2.5 km for the Prelitoral and Litoral ranges, respectively. The exhumation history of these samples is depicted in Figure 10. Figure 11 shows their thermal history as derived from the upper crustal model, as well as the thermal history when assuming an extra increase in the geothermal gradient of 11°C/km from the Neogene onward, as derived from the lithospheric-scale model.

6.1.1. Prelitoral Synthetic Sample

[51] The sample outcropping in the Prelitoral Range is presently located in the frontal part of the CIC and in the footwall of the Vallès-Penedès Fault (VPf in Figure 8). It was considered to be initially located at a depth of 3.6 km (at 55 Ma), corresponding to a modeled temperature of around 80°C. The predicted Paleogene thermal history for this sample (Figure 11) shows a slight temperature decrease during the Eocene-early Oligocene (±10°C from 55 to 28 Ma). This cooling is related to tectonic uplift of the CIC (coeval to the motion of thrusts Th1 and Th2) which generated a positive relief that was counteracted by erosion of 1.3 km. It should be noted, however, that in the model the hanging wall movement along Th2 is hardly registered by this sample, owing to its location in the shear zone of the fault. In the model, this is the narrow zone between the moving grid points of the hanging wall and the static grid points in the footwall.

[52] During the extensional stage (28–0 Ma), the model shows a fast, significant temperature decrease of the modeled sample until the surface temperature (Figure 11). This is the result of the unroofing of the uplifted footwall block of the Vallès-Penedès Fault (i.e., the Prelitoral Range), which rebounded flexurally [*Gaspar-Escribano et al.*, 2004]. The influence of the lithospheric thinning in the Valencia Trough from the Neogene onward on the modeled T-t signal is insignificant. This is due to the fact that the resulting rise in the geothermal gradient causes an absolute temperature difference that increases with time and with depth, but is coeval with the exhumation of the sample. In the time that the gradient increases with 11°C/km, as was calculated from the lithsopheric-scale model, the sample travels upward from 2.3 to 0 km. At 2.3 km the increase in T would be 25.3 degrees, but at the time this temperature is reached at this depth, the sample has already arrived at the surface.

6.1.2. Litoral Synthetic Sample

[53] The modeled sample from the present-day Litoral Range was located at a depth of 2.5 km (Figure 10) with a modeled temperature of ~55°C (Figure 11) at the commencement of the compressional phase (~55 Ma). In contrast with the prelitoral synthetic sample, modeling results show noticeable changes in the thermal history during compression, with two well-differentiated stages. The first, coeval to the activation of the Th1-thrust, (early middle Eocene; 55–41 Ma) is characterized by reheating of the litoral sample as a result of deposition (burial) of more than 0.8 km of sediments in the hinterland areas (Figure 10). The second one is related to emplacement of the out-of-sequence thrust (Th2) during the late Eocene–early Oligocene (41–29 Ma), which generated a widening of the

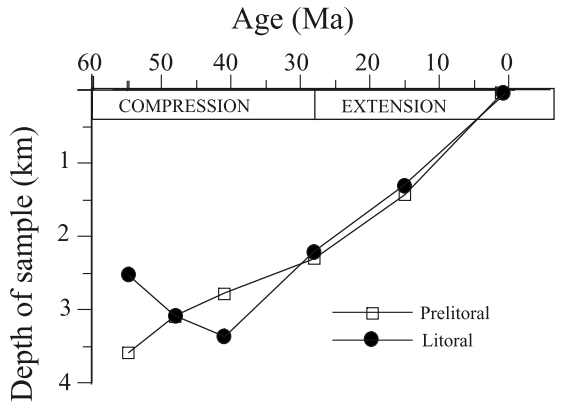

Figure 10. Depth (relative to Earth surface) versus age diagrams for the two synthetic samples shown in Figure 8, representing prelitoral and litoral range.

uplifted areas of the CIC toward the SE and as a consequence the uplift of the litoral sample. This produced a sample exhumation of 1.2 km (including the 0.8 km of sediments deposited previously) and is reflected by the cooling pulse predicted for this period (Figure 11).

[54] Later, during the extensional stage (28–0 Ma), uplift of the Barcelona Fault footwall block due to flexural rebound and its consequent unroofing implied an exhumation of nearly 2.3 km of the Litoral Range (Figure 10). The influence of Neogene rifting in the Valencia Through does not change this conclusion, since, similar to the prelitoral sample, the litoral sample travels upward during the resulting increase in geothermal gradient, thereby escaping from significant heating.

6.2. AHe Ages of the Synthetic Rock Samples

[55] The T-t paths resulting from the combined modeling results, including both the large-scale and the crustal-scale signal, were imported into DECOMP (A Bikker et al., DECOMP.1.1, 2002, FALW, Vrije Universiteit, Amsterdam) [*Meesters and Dunai*, 2002], in order to calculate the corresponding AHe ages. For this DECOMP-modeling we described our samples as a sphere with a radius of 72 μm, since this has an equivalent volume-to-surface radius as a hexagonal prism with a radius/length of 61/227 μm, which is the average grain size of our samples. Further assuming Do = 50 $cm^2\ s^{-1}$, E_a = 33.5 kcal mol^{-1} [*Farley*, 2000], (where D_0 = the diffusivity at T = ∞ and E_a = activation energy), and a homogenous parent element distribution, we found modeled AHe ages of 25 Ma for both samples.

6.3. Comparison Between Modeling Results and Thermochronological Data

6.3.1. Paleogene

[56] The calculated Paleogene thermal history for the modeled samples is consistent with the thermochronological data within the error margins (Figure 11), with the exception of the basement temperature increase predicted in the hinterland of the CIC (Litoral Range sample location) from about 55 to 41 Ma. In the model, this event is related to the deposition of sediments above the sample in a piggyback depositional setting. However, analyses of the sedimentary record of the Barcelona Basin reveal that hinterland sedimentation was restricted to the present-day offshore and furthermore suggest that it did not commence before late Eocene [*Roca et al.*, 1999; *Roca*, 2001]. Thus the area corresponding to the present-day Litoral Range must have been a topographic high during the entire compressive stage.

[57] The difference between this inferred topography and the modeled one might be related to a change of the Th1 thrust geometry in depth, not included in the model, or to an inclined shear deformation style rather than the vertical shear assumed by the model. This would result in a widening of the uplifted area. Under such a setting, the predicted thermal history would not show a significant reheating pulse (as in Figure 11) but a constant temperature profile or a mild cooling trend. Again, another possibility is the existence of another Paleogene thrust fault (Th3 in Figure 8) which might have uplifted the area where the Litoral Range is located at Present, thereby facilitating hinterland sedimentation (consistently with the modeled thermal trends). However, the existence of such a fault is highly speculative. This hypothesis is discussed more extensively by *Gaspar-Escribano et al.* [2004]. For the Prelitoral Range, calculated amounts of basement material exhumed during Paleogene are comparable to constraints on erosion from the sedimentary record ($\sim$0.8 km [*López-Blanco et al.*, 2000]).

6.3.2. Neogene

[58] Thermal histories derived from modeling results for the extensional phase show a period of Neogene cooling (Figure 11). These predictions are in accordance with AFT thermal histories of samples [4], [67] and [135] (section 3), indicating cooling from temperatures around the upper bench mark of the AFT partial annealing zone ($\sim$60°C), and is interpreted as a consequence of almost 2.5 km of erosion of elevated areas in the CCR.

[59] In turn, our model cannot reproduce any thermal scenario for AFT samples [36], [106] and [137] (section 3), which are shown to cool from temperatures in excess of $\sim$110°C during the extensional phase. This would imply erosion of more than 4 km of rocks based on the $\sim$24°C/km gradient calculated by our model (Figure 9). However, such an amount of erosion is unrealistically high considering the regional stratigraphy of the uplifted areas and the volume of sediments (<3 km thick) infilling the Vallès-Penedès Basin. Neither the modeling predictions nor the irregular geographical pattern of reset AFT cooling ages support exhumational cooling. Hence these samples are likely to record local thermal overprinting due to locally increased geotherms, caused by a mechanism not considered in our model. Since the samples concerned were positioned less than 2.5 km deep at the beginning of our model, a syn-extensional (late Oligocene–Neogene) geothermal gradient of more than 40°C/km is needed to explain the temperatures of more than 110°C.

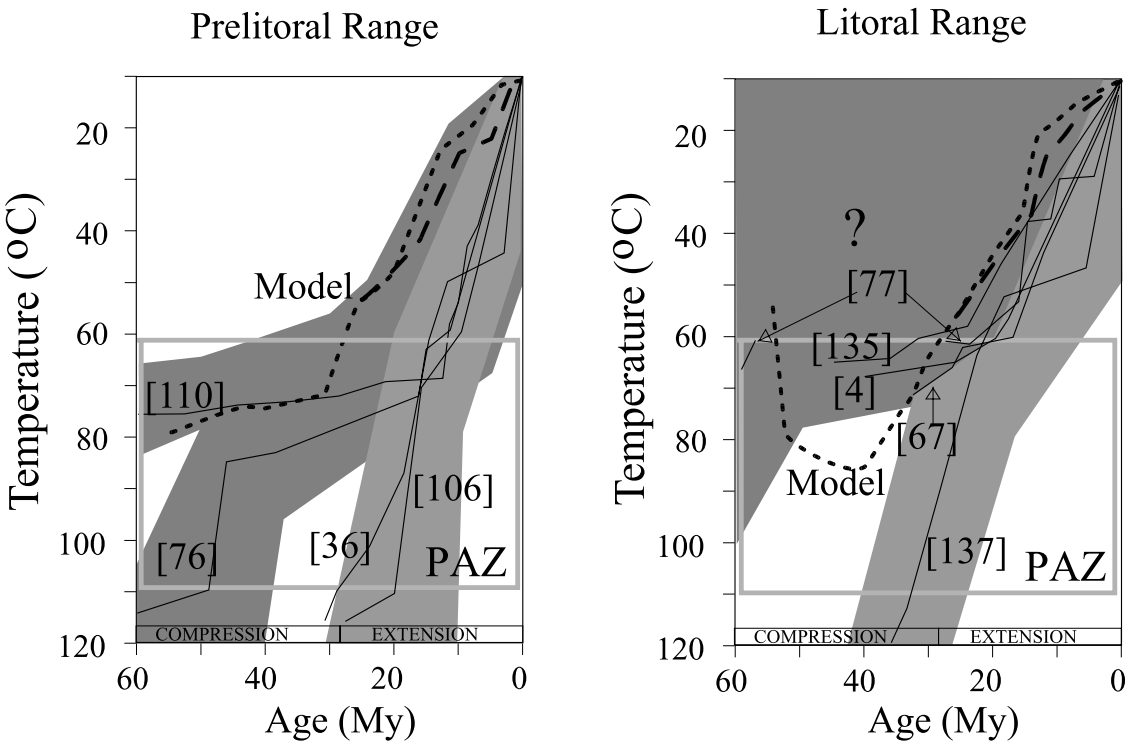

Figure 11. Comparison between numerical modeling results (dashed lines) and thermal histories derived from AFT thermal modeling (solid lines) for the prelitoral (left) and litoral ranges (right). Short dashes denote results of the upper crustal–scale model. Long dashes denote results of the upper crustal–scale model combined with the increase in gradient as derived from the lithospheric-scale model. Black solid lines are best fit AFT-derived thermal histories. Gray shading denotes error bands of AFT derived thermal histories. Numbers correspond to different samples (see location in Figure 4). Gray box is temperature interval constrained by the AFT thermochronometers (i.e., the partial annealing zone, PAZ).

6.3.3. Possible Explanations for Elevated Geotherms

[60] The confined elevated geothermal gradients revealed from our analysis could be related to three not modeled mechanisms: (1) magmatism, (2) frictional heat along the fault planes, and/or (3) heat convection driven by groundwater flow.

[61] 1. The local magmatic source can be ruled out because of the absence of Cenozoic magmatic occurrences in the CCR. Syn-extensional Neogene magmatic outcrops are present close to the CCR [*Tassone et al.*, 1996], but these magmatic manifestations were very restricted in time and space and therefore incapable to produce the observed geothermal anomalies.

[62] Also neither the major lithospheric thinning in the Valencia Trough, neither a subcrustal control related to late Neogene magmatic activity northeastward of the CCR can be regarded as a source of the thermal gradient anomalies. Not only because the thinning event is shown to have a very limited effect on the temperature-time curves, but also because these heat sources both would affect all samples located in the Catalan margin and not only a few of them. Such a scenario is not capable to explain the pattern of geothermal anomalies observed in the Catalan margin [*Fernàndez et al.*, 1990a, 1998].

[63] 2. *Fernàndez and Banda* [1990] calculated the effect of frictional heat for the main Neogene extensional faults in the CCR. Assuming a rate of fault movement of 1 mm/a, they estimated a temperature increase in the fault plain between 1° and 5°C at 0–3 km depth. Hence they concluded that frictional heat led to no significant temperature changes even for rocks close to the fault plain. Despite the fact that higher temperatures up to 100°C might be reached by higher slip rates of 10–100 mm/a, and for high shear resistance exceeding 100 MPa [*Sibson*, 1983], temperature changes on the fault plain typically last for a very short time and cause no effect on the apatite fission track record [*D'Alessio et al.*, 2003].

[64] 3. Heat convection by groundwater flow [e.g., *Swanberg*, 1983; *Bodri*, 1994; *Bodri and Rybach*, 1998] can have a strong effect on the geothermal gradient, and is shown to be able to cause a difference of a factor 2 in geothermal gradients between recharge and discharge areas [*Person et al.*, 1995]. This mechanism has been invoked by *Fernàndez and Banda* [1989, 1990] to explain the present-day local geothermal anomalies reported along some of the main extensional faults and in the axial region of the Valencia Through. They proposed a model of topography-driven flow (forced convection) in which meteoric waters

percolate through the elevated footwall areas to deep levels and come back to the surface following fault planes (e.g., NE segment of the Vallès-Penedès Fault [*Fernàndez and Banda*, 1990]). This hypothesis has been successfully verified by numerical modeling studies implicitly incorporating heat transport and fluid flow equations, yielding variations in temperatures of several tens of degrees at shallow depths (up to 3 km) due to groundwater flow, and has been applied to several locations in the CCR [*Fernàndez et al.*, 1990b, 1998; *Carmona et al.*, 2000; *Bitzer et al.*, 2001].

[65] On the basis of AFT and AHe results, *Juez-Larré and Andriessen* [2006] proposed that a similar forced convection mechanism might have played an active role in the thermal history of certain rocks during the Neogene phase of extension. Despite the uncertainty of the AFT thermal modeling, which does not allow distinguishing in which phase of extension cooling took place, we consider likely that cooling occurred only after the generation of important topography, therefore well into the phase of extension. Mineralogical and geochemical study of the vein system yield evidence for syn-extensional fluid circulation [*Cardellach et al.*, 2002], with hot fluids reaching temperatures of 80°–150°C, and in some veins even up to 230°C. On the basis of all the above arguments, we surmise that heat convection is the most likely heat convection mechanism to have increased the temperature of basement rocks located close to the major extensional faults, and could account for the local temperature increment which reset some AFT thermochronometers.

7. Conclusions

[66] Several processes affecting the geothermal field are analyzed in this paper through a scale-bridging approach integrating a variety of data sources and thermo-kinematic modeling. By establishing a division between processes operating at different wavelengths, we were able to distinguish amongst various sources contributing to the geothermal field.

[67] We show that the thermal field of an intraplate chain is hardly influenced by the effect of the fault block movements, but rather by erosion of the positive relief created by thrusting. Thermal changes are even more significant in areas flanking rift basins, where contributions from both deep and shallow sources add up. We demonstrate that mass redistribution (erosion and deposition) of the rift flanks have a first-order effect on the thermal evolution of rift flanks, eventually implying larger thermal changes than those related to variations in lithospheric thickness and upwelling of relatively hot asthenospheric material. Other elements potentially controlling the geothermal field, such as fluid convection, can be at least of similar importance at very local scales.

[68] For the case of the central Catalan Coastal Ranges, our results support the following scenario for their Cenozoic thermal evolution: During the Paleogene compressional phase, the geothermal gradient did not experience significant variations in the uppermost crust due to thrusting and subsequent erosion; cooling of rock samples can generally be explained as denudation. During the Neogene, lithospheric thinning in the Valencia Trough implies a general narrowing of the spacing between isotherms, and consequently a rise in geothermal gradient. The estimated increase is 11°C/km for the uppermost levels of the Catalan Coastal Ranges. This overall heating, however, is hardly recorded by the relatively shallow samples used for thermochronological data in the study area, and cannot account for the differential Neogene cooling histories recorded by the AFT results. Since also no relevant differences in erosional patterns of samples are found within the studied area, we support the idea that forced fluid convection locally increased the geothermal gradient, especially in the vicinity of the major extensional fault planes.

[69] The coupling of lithospheric and crustal scales for the analysis of thermal processes as demonstrated in this paper adds to earlier work focusing on coupling of scales for flexural processes [*ter Voorde et al.*, 1997; *Gaspar-Escribano*, 2003]. This modeling approach, comprising not only different scales but also different tectonic environments in the same area, is innovative and can be exported to the analysis of other intraplate chains submitted to compressive tectonics and of rift basin flanks. In this context, thermochronological data are extremely useful in arising arguments for supporting or disregarding the occurrence of various processes causing heat redistribution in the crust.

[70] **Acknowledgments.** This paper is publication 20070606 of the Netherlands Research School of Sedimentary Geology (NSG) and it has been financed by: (1) the Earth and Life Sciences (ALW) Council of the Netherlands Organization for Scientific Research (NWO); (2) the Spanish Science and Technology Ministry (MCYT; project CGL2004-05816-C02-01); and (3) the Research Group of Geodynamics and Basin Analysis (2005SGR00397) from the Generalitat de Catalunya. Constructive reviews of Jurgen Foeken and Ulrich Glasmacher are highly appreciated.

References

Ayala, C., J. Pous, and M. Torné (1996), The lithosphere-asthenosphere boundary of the Valencia trough (western Mediterranean) deduced from 2D geoid and gravity modeling, *Geophys. Res. Lett.*, *23*, 3131–3134.

Ayala, C., M. Torné, and J. Pous (2003), The lithosphere-asthenosphere boundary in the western Mediterranean from 3D joint gravity and geoid modeling: Tectonic implications, *Earth Planet. Sci. Lett.*, *209*, 275–290.

Banda, E. (1988), Crustal parameters in the Iberian Peninsula, *Phys. Earth Planet. Inter.*, *51*, 222–225.

Bartrina, M. T., L. Cabrera, M. J. Jurado, J. Guimerà, and E. Roca (1992), Evolution of the central Catalan margin of the Valencia trough (western Mediterranean), *Tectonophysics*, *203*, 219–247.

Bitzer, K., A. Travé, and J. M. Carmona (2001), Fluid flow processes at basin scale, *Acta Geol. Hisp.*, *36*, 1–20.

Bodri, B. (1994), Hydrological disturbances of the conductive heat flow in stable continental crust, *Tectonophysics*, *234*, 291–304.

Bodri, B., and L. Rybach (1998), Influence of topographically driven convection on heat flow in the Swiss Alps: A model study, *Tectonophysics*, *291*, 19–27.

Cabrera, L., and F. Calvet (1996), Onshore Neogene record in NE Spain: Vallès-Penedès and El Camp half-grabens (NW Mediterranean), in *Tertiary Basins of Spain*, edited by P. F. Friend and C. J. Dabrio, pp. 97–105, Cambridge Univ. Press, Cambridge, U.K.

Cardellach, E., A. Canals, and F. Grandia (2002), Recurrent hydrothermal activity induced by successive extensional episodes: the case of the Berta

F-(Pb-Zn) vein system (NE Spain), *Ore Geol. Rev.*, *22*, 133–141.

Carmona, J. M., K. Bitzer, E. López, and M. Bouazza (2000), Isotopic composition and origin of geothermal waters at Caldetes (Maresme-Barcelona), *J. Geochem. Explor.*, *69*, 441–447.

Clavell, E., and X. Berástegui (1991), Petroleum geology of the Gulf of Valencia, in *Generation, Accumulation and Production of Europe's Hydrocarbons*, edited by A. M. Spencer, pp. 355–368, Oxford Univ. Press, Oxford, U.K.

D'Alessio, M. A., A. E. Blythe, and R. Bürgman (2003), No frictional heat along the San Gabriel fault, California: Evidence from fission-track thermochronology, *Geology*, *31*(6), 541–544.

Drogue, C. (1985), Geothermal gradients and ground water circulation in fissured and karstic rocks: The role played by the structure of the permeable network, *J. Geodyn.*, *4*, 219–231.

Durand, B. (Ed.) (1984), *Thermal Phenomena in Sedimentary Basins*, *Collect. Colloq. Seminaires*, vol. 41, 326 pp., Technip, Paris.

Ehlers, T. A., and D. S. Chapman (1999), Normal fault thermal regimes: Conductive and hydrothermal heat transfer surrounding the Wasatch fault, Utah, *Tectonophysics*, *312*, 217–234.

Ehlers, T. A., and K. Farley (2003), Apatite (U-Th)/He thermochronology: Methods and applications to problems in tectonic and surface processes, *Earth Planet. Sci. Lett.*, *206*, 1–14.

Farley, K. A. (2000), Helium diffusion from apatite: General behavior as illustrated by Durange fluorapatite, *J. Geophys. Res.*, *105*, 2903–2914.

Fernàndez, M., and E. Banda (1989), An approach to the thermal field in northeastern Spain, *Tectonophysics*, *164*, 259–266.

Fernàndez, M., and E. Banda (1990), Geothermal anomalies in the Vallès-Penedès graben master fault: Convection through the horst as a possible mechanism, *J. Geophys. Res.*, *95*, 4887–4894.

Fernàndez, M., M. Torné, and H. Zeyen (1990a), Lithospheric thermal structure of NE Spain and the north-Balearic basin, *J. Geodyn.*, *12*, 253–267.

Fernàndez, M., M. Torné, and H. Zeyen (1990b), Modelling of thermal anomalies in the NW border of the Valencia Trough by ground water convection, *Geophys. Res. Lett.*, *17*, 105–108.

Fernàndez, M., I. Marzán, A. Correia, and E. Ramalho (1998), Heat flow, heat production, and lithospheric thermal regime in the Iberian Peninsula, *Tectonophysics*, *291*, 29–53.

Fontboté, J. M., J. Guimerà, E. Roca, F. Sàbat, P. Santanach, and F. Fernández-Ortigosa (1990), The Cenozoic evolution of the Valencia Trough (western Mediterranean), *Rev. Soc. Geol. Esp.*, *3*, 249–259.

Gallagher, K., R. Brown, and C. Johnson (1998), Fission-track analysis and its application to geological problems, *Annu. Rev. Earth Planet. Sci.*, *26*, 1229–1236.

Gallart, J., N. Vidal, J. J. Dañobeitia, and the ESCI-Valencia Trough Working Group (1994), Lateral variations in the deep crustal structure at the Iberian margin of the Valencia trough imaged from seismic reflection methods, *Tectonophysics*, *232*, 59–75.

Gaspar-Escribano, J. M. (2003), Tectonic modeling of the Catalan Coastal Ranges (NE Spain) and adjacent areas, Ph.D. thesis, 140 pp., Vrije Univ., Amsterdam.

Gaspar-Escribano, J. M., J. D. van Wees, M. ter Voorde, S. Cloetingh, E. Roca, L. Cabrera, J. A. Muñoz, P. A. Ziegler, and D. Garcia-Castellanos (2001), 3D flexural modeling of the Ebro Basin (NE Iberia), *Geophys. J. Int.*, *145*, 349–367.

Gaspar-Escribano, J. M., M. ter Voorde, E. Roca, and S. Cloetingh (2003), Mechanical (de-) coupling of the lithosphere in the Valencia Trough (NW Mediterranean): What does it mean?, *Earth Planet. Sci. Lett.*, *210*, 291–303.

Gaspar-Escribano, J. M., D. Garcia-Castellanos, E. Roca, and S. Cloetingh (2004), Cenozoic vertical motions of the Catalan Coastal Ranges (NE Spain): The role of isostasy, fault tectonics and surface transport, *Tectonics*, *23*, TC1004, doi:10.1029/2003TC001511.

Grasemann, B., and N. S. Mancktelow (1993), Two-dimensional thermal modelling of normal faulting: The Simplon Fault Zone, Central Alps, Switzerland, *Tectonophysics*, *225*, 155–165.

Guimerà, J. (1988), Estudi structural de l'enllaç entre la Serralada Ibèrica i la Serralada Costanera Catalana, Ph.D. thesis, 600 pp., Univ. de Barcelona, Barcelona, Spain.

Haq, B. U., J. Hardenbol, and P. R. Vail (1987), Chronology of fluctuating sea levels since the Triassic, *Science*, *235*, 1156–1167.

Janssen, M. E., M. Torné, S. Cloetingh, and E. Banda (1993), Pliocene uplift of the eastern Iberian margin: Inferences from quantitative modelling of the Valencia Trough, *Earth Planet. Sci. Lett.*, *119*, 585–597.

Juez-Larré, J. (2003), Post Late Paleozoic tectonothermal evolution of the northeast margin of Iberia, assessed by fission-track and (U-Th)/He analysis, Ph.D. thesis, 200 pp., Vrije Univ., Amsterdam.

Juez-Larré, J., and P. A. M. Andriessen (2002), Post Late Paleozoic tectonism in the southern Catalan Coastal Ranges (NE Spain), assessed by apatite fission-track analysis, *Tectonophysics*, *349*, 113–129.

Juez-Larré, J., and P. A. M. Andriessen (2006), Tectonothermal evolution of the northeastern margin of Iberia since the break-up of Pangea to present, revealed by low-temperature fission-track and (U–Th)/He thermochronology: A case history of the Catalan Coastal Ranges, *Earth Planet. Sci. Lett.*, *243*, 159–180.

Ketcham, R. A., R. A. Donelick, and M. B. Donelick (2000), AFTSolve: A program for multi-kinetic modeling of apatite fission-track data, *Geol. Mater. Res.*, *2*, 1–32.

Kooi, H., S. Cloetingh, and J. Burrus (1992), Lithospheric necking and regional isostasy at extensional basins: 1. Subsidence and gravity modeling with application to the Gulf of Lions margin (SE France), *J. Geophys. Res.*, *97*, 17,553–17,571.

Kukkonen, I. T. (1995), Thermal aspects of groundwater circulation in bedrock and its effect on crustal geothermal modelling in Finland, the central Fennoscandian Shield, *Tectonophysics*, *244*, 119–136.

Laslett, G. M., P. F. Green, I. R. Duddy, and A. J. W. Gleadow (1987), Thermal annealing of fission-tracks in apatite, 2. A quantitative analysis, *Chem. Geol.*, *65*, 1–13.

López-Blanco, M. (2002), Sedimentary response to thrusting and fold growing on the SE margin of the Ebro basin (Paleogene, NE Spain), *Sediment. Geol.*, *146*, 133–154.

López-Blanco, M., M. Marzo, D. W. Burbank, J. Vergés, E. Roca, P. Anadón, and J. Piña (2000), Tectonic and climatic controls on the development of foreland fan deltas: Monserrat and Sant Llorenç del Munt systems (Middle Eocene, Ebro Basin, NE Spain), *Sediment. Geol.*, *138*, 17–39.

Martí, J., J. Mitjavila, E. Roca, and A. Aparicio (1992), Cenozoic magmatism of the Valencia trough (western Mediterranean): relationships between structural and volcanism, *Tectonophysics*, *203*, 145–165.

Marzo, M., and P. Anadón (1988), Anatomy of a conglomeratic fan-delta complex: The Eocene Monserrat conglomerate, Ebro Basin, northeastern Spain, in *Fan Deltas: Sedimentology and Tectonic Settings*, edited by W. Nemec and R. J. Steel, pp. 319–340, Blackie and Son, Glasgow, U.K.

McKenzie, D. (1978), Some remarks on the development of sedimentary basins, *Earth Planet. Sci. Lett.*, *40*, 25–32.

Meesters, A., and T. Dunai (2002), Solving the production-diffusion equation for finite diffusion domains of various shapes. II: Application to cases with alpha-ejection and non-homogeneous distribution of the source, *Chem. Geol.*, *186/3–4*, 351–369.

Morency, C., M. P. Doin, and D. Dumoulin (2002), Convective destabilization of a thickened continental lithosphere, *Earth Planet. Sci. Lett.*, *202*, 303–320.

Morgan, P., and M. Fernàndez (1992), Neogene vertical movements and constraints on extension in the Catalan Coastal Ranges, Iberian Peninsula, and Valencia Trough, Western Mediterranean, *Tectonophysics*, *203*, 185–201.

Negredo, A. M., M. Fernàndez, M. Torné, and C. Doglioni (1999), Numerical modeling of simultaneous extension and compression: The Valencia Trough (western Mediterranean), *Tectonics*, *18*, 361–374.

Parcerisa, D., D. Gómez-Gras, E. Roca, J. Madurell, and J. Agustí (2007), The Upper Oligocene of Montgat (Catalan Coastal Ranges, Spain): New age constraints to the western Mediterranean Basin opening, *Geol. Acta*, *5*(1), 3–17.

Person, M., D. Toupin, and P. Eadington (1995), One-dimensional models of groundwater flow, sediment thermal history and petroleum generation within continental rift basins, *Basin Res.*, *7*, 81–96.

Pino, N. A., and D. V. Helmberger (1997), Upper mantle compressional velocity structure beneath the West Mediterranean basin, *J. Geophys. Res.*, *102*, 2953–2967.

Rahn, M. K., and B. Grasemann (1999), Fission-track and numerical thermal modeling of differential exhumation of the Glarus thrust plane (Switzerland), *Earth Planet. Sci. Lett.*, *169*, 245–259.

Ring, U., M. T. Brandon, G. S. Lister, and S. Willett (1999), Exhumation processes, in *Exhumation Processes: Normal Faulting, Ductile Flow and Erosion*, edited by U. Ring et al., *Geol. Soc. Spec. Publ.*, *154*, 1–28.

Roca, E. (1996), La evolución geodinámica de la Cuenca Catalano-Balear y áreas adyacentes desde el Mesozoico hasta la actualidad, *Acta Geol. Hisp.*, *29*, 3–25.

Roca, E. (2001), The Northwest-Mediterranean basin (Valencia Trough, Gulf of Lions and Liguro-Provençal basins): Structure and geodynamic evolution, in *Peri Tethyan Rift/Wrench Basins and Passive Margins*, *PeriTethys Mem.*, vol. 6, edited by P. A. Ziegler et al., pp 671–706, Mus. Natl. d'Histoire Nat., Paris.

Roca, E., and P. Desegaulx (1992), Analysis of the geological evolution and vertical movements in the Valencia Trough (western Mediterranean), *Mar. Pet. Geol.*, *9*, 167–185.

Roca, E., and J. Guimerà (1992), The Neogene structure of the eastern Iberian margin: structural constraints on the crustal evolution of the Valencia Trough (western Mediterranean), *Tectonophysics*, *203*, 203–218.

Roca, E., M. Sans, L. Cabrera, and M. Marzo (1999), Oligocene to Middle Miocene evolution of the Central Catalan margin (North-western Mediterranean), *Tectonophysics*, *315*, 209–229.

Roca, E., D. Frizon de Lamotte, A. Mauffret, R. Bracène, J. Vergés, N. Benaouali, M. Fernàndez, J. A. Muñoz, and H. Zeyen (2004), TRANSMED Transect II, in *The Transmed Atlas—The Mediterranean Region from Crust to Mantle* [CD-ROM], edited by W. Cavazza et al., Springer, Berlin. (Also available at http://hal.ccsd.cnrs.fr/ccsd-00069583/en/)

Sàbat, F., E. Roca, J. A. Muñoz, J. Vergés, P. Santanach, M. Sans, E. Masana, A. Estévez, and C. Santisteban (1997), Role of extension and compression in the evolution of the eastern margin of Iberia: The ESCI-Valencia Trough seismic profile, *Rev. Soc. Geol. Esp.*, *8*, 431–448.

Sibson, R. H. (1983), Continental fault structure and the shallow earthquake source, *J. Geol. Soc.*, *140*, 741–767.

Stüwe, K., L. White, and R. Brown (1994), The influence of eroding topography on steady-state isotherms: Application to fission-track analysis, *Earth Planet. Sci. Lett.*, *124*, 63–74.

Swanberg, C. A. (1983), Geothermal resources of rifts: A comparison of the Rio Grande Rift and Salton Trough, *Tectonophysics*, *94*, 659–678.

Tassone, A., E. Roca, J. A. Muñoz, L. Cabrera, and M. Canals (1996), Evolución del sector septentrional del margen continental catalán durante el Cenozóico, *Acta Geol. Hisp.*, *29*, 3–38.

ter Voorde, M. (1996), Tectonic modelling of lithospheric extension along faults: Implications for ther-

mal and mechanical structure and basin stratigraphy, Ph.D. thesis, 197 pp., Vrije Univ., Amsterdam.

ter Voorde, M., and G. Bertotti (1994), Thermal effects of normal faulting during rifted basin formation, 1. A finite difference model, *Tectonophysics*, *240*, 133–144.

ter Voorde, M., R. Ravnås, R. Færseth, and S. Cloetingh (1997), Tectonic modelling of the Middle Jurassic synrift stratigraphy in the Oseberg-Brage area, northern Viking Graben, *Basin Res.*, *9*, 133–150.

ter Voorde, M., R. t. Van Balen, G. Bertotti, and S. A. P. L. Cloetingh (1998), The influence of a stratified rheology on the flexural response of the lithosphere to (un)loading by extensional faulting, *Geophys. J. Int.*, *134*, 721–735.

ter Voorde, M., C. H. de Bruijne, S. A. P. L. Cloetingh, and P. A. M. Andriessen (2004), Thermal consequences of thrust faulting: Simultaneous versus successive fault activation and exhumation, *Earth Planet. Sci. Lett.*, *223*, 395–413.

Vidal, N., J. Gallart, and J. J. Dañobeitia (1998), A deep seismic crustal transect from the NE Iberian Peninsula to the western Mediterranean, *J. Geophys. Res.*, *103*, 12,381–12,396.

Vlaar, N. J. (1983), Thermal anomalies and magmatism due to lithospheric doubling and shifting, *Earth Planet. Sci. Lett.*, *65*, 322–330.

Watts, A. B., and M. Torné (1992), Subsidence history, crustal structure and thermal evolution of the Valencia Trough: A young extensional basin in the Western Mediterranean, *J. Geophys. Res.*, *97*, 20,021–20,041.

Zeyen, H., and M. Fernàndez (1994), Integrated lithospheric modeling combining thermal, gravity and local isostasy analysis: Application to the NE Spanish geotransect, *J. Geophys. Res.*, *99*, 18,089–18,102.

P. Andriessen, S. Cloetingh, J. Juez-Larré, and M. ter Voorde, Faculty of Earth and Life Sciences, Vrije Universiteit, De Boelelaan 1085, 1081 HV, Amsterdam, Netherlands. (marlies.ter.voorde@falw.vu.nl)

J. M. Gaspar-Escribano, ETSI Topografía, Geodesia y Cartografía, Universidad Politécnica de Madrid, Ctra. de Valencia km 7, E-28031 Madrid, Spain.

E. Roca, Facultat de Geologia, Universitat de Barcelona, c/Martí Franquès, s/n, E-08028 Barcelona, Spain.